LLNL Pure Positron Plasma Program

J. H. Hartley, B. R. Beck, T. E. Cowan, J. Fajans, R. Gopalan,
R. H. Howell, J. L. McDonald, R. R. Rohatgi

Lawrence
Livermore
National
Laboratory

LLNL Pure Positron Plasma Program

J.H. Hartley[§], B.R. Beck[†], T.E. Cowan[†], J. Fajans[‡], R. Gopalan[‡], R.H. Howell[†], J.L. McDonald[†], and R.R. Rohatgi[†]

[†]*Physics Department and* [§]*U.C. Davis Department of Applied Science, Lawrence Livermore National Laboratory, Livermore, CA 94551*
[‡]*Physics Department, University of California, Berkeley, CA, 94720*

Abstract. Assembly and initial testing of the Positron Time-of-Flight Trap at the Lawrence Livermore National Laboratory (LLNL) Intense Pulsed Positron Facility has been completed. The goal of the project is to accumulate a high-density positron plasma in only a few seconds, in order to facilitate study that may require destructive diagnostics. To date, densities of at least 6×10^6 positrons per cm^3 have been achieved.

TRAP DESIGN

The LLNL pure plasma trap has an unusual configuration for a non-neutral plasma device, which was driven by its intended use as a high-density positron gas target for particle physics experiments (1). The positron trap consists of a 76 cm long cylindrical-electrode Penning-Malmberg trap in a high-uniformity solenoid capable of producing a 62 kG axial magnetic field. The apparatus is situated on the positron beam line of the LLNL 100 MeV electron Linac.

At the time of the design, the conventional wisdom in non-neutral traps was that azimuthal asymmetries of the field and electrodes were a major limiting factor to the plasma confinement time (2). For this reason, great care was taken to ensure that the solenoid field was very uniform, and that the electrodes were aligned with great precision. The measured field strength varies by less than 0.1% axially over the length of the trap, and ~20 ppm peak-to-peak azimuthally at the electrode radius of 1 cm (Fig. 1). The size and radial dependence of the asymmetries in the field can be accounted for by a horizontal 0.125 mm bow in the 1 m long coil, resulting in a toroidal field with a radius of curvature of 1 km.

The electrodes are gold-plated copper cylinders aligned in a ceramic V-block cradle. All components are machined to 2.5 μm tolerance over the length of the trap. The trap structure is situated in a copper bore whose temperature can be varied from 300 K to 4.2 K.

The primary plasma diagnostic consists of a micro-channel plate (MCP) in front of a phosphor screen, imaged by a CCD camera. Camera images are captured on a VAX Workstation.
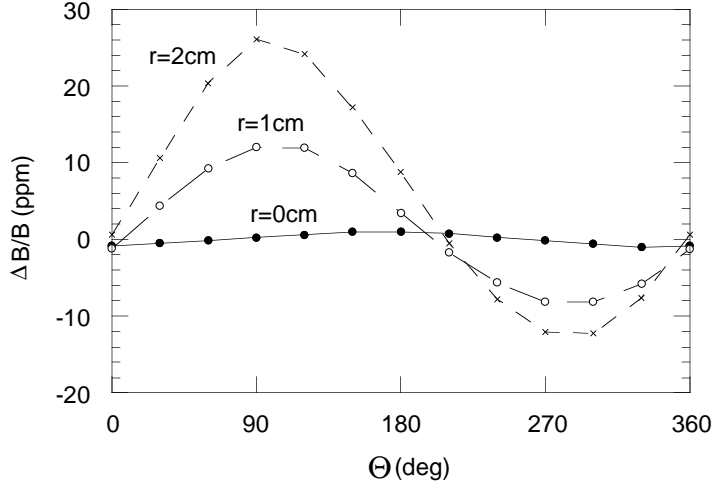
Figure 1. Magnetic field variation with azimuthal angle at three radii. 0° and 180° define the vertical plane.

OPERATION WITH ELECTRON PLASMAS

Preliminary testing of the trap utilized electrons from a spiral filament as the plasma particles. The trap region was 6 cm long, with B=30 kG and T=77 K. Plasma density measurements were made by dumping the plasma from the trap onto a phosphor screen. The radial density profile was determined from the image intensity and a capacitive pick-off of the total charge on the screen.

At the time of our initial measurements, summarized in Figures 2 and 3, the CCD camera imaging system was not yet operational, so human eyes and a ruler were used to measure the diameter of the plasma. Work done at UC San Diego (3) and UC Berkeley (4), and the qualitative appearance of the phosphor image, suggested that assuming flat profile would be a reasonable approximation and that the calculated average density was adequate to characterize the plasma expansion.

The plasma underwent an early stage of rapid transport, followed by a much slower expansion. This was consistent with the behavior of other non-neutral plasma devices, and suggested a quick evolution of the radial profile to an equilibrium flat distribution. The data was fit as two exponentials, and the t=0 equilibrium density was defined to be the intercept of the second, slower exponential with the y axis. Confinement time was defined as the time it took for the average density to drop to one-half of the equilibrium density.

With the bore at room temperature, confinement times were on the order of ten seconds. With the bore cooled to 77 K, lifetimes improved to as much as several thousand seconds. This factor of 100 difference is presumed to result from the improvement in vacuum pressure due to cryopumping. Pressure measured well outside the cryopumping region improved from 2×10^{-9} to 2×10^{-10} Torr with cooling, and the improvement was likely much greater in the trap region.

Earlier work (5) has suggested that the lifetime scaling should follow:

$$\tau_m \propto \frac{B^2}{L^2} \cdot \frac{1}{P} \cdot \frac{f(T)}{n^a}, \qquad (1)$$
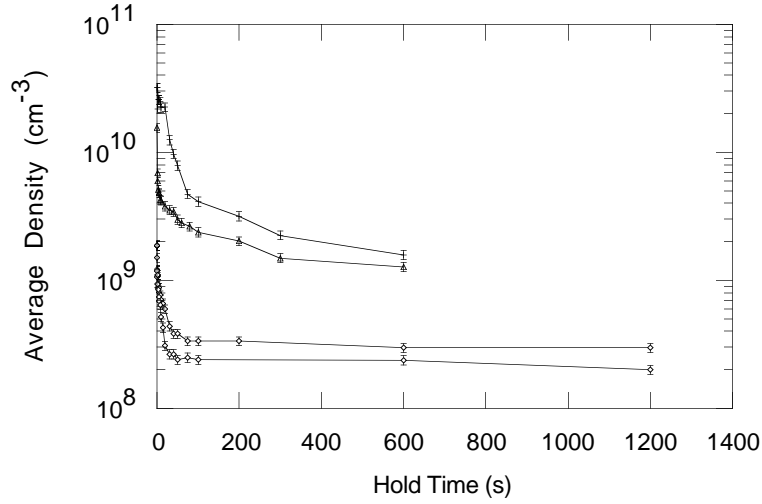
Figure 2. Electron average density as a function of hold time. (L=6 cm, B=30 kG, T=77 K)
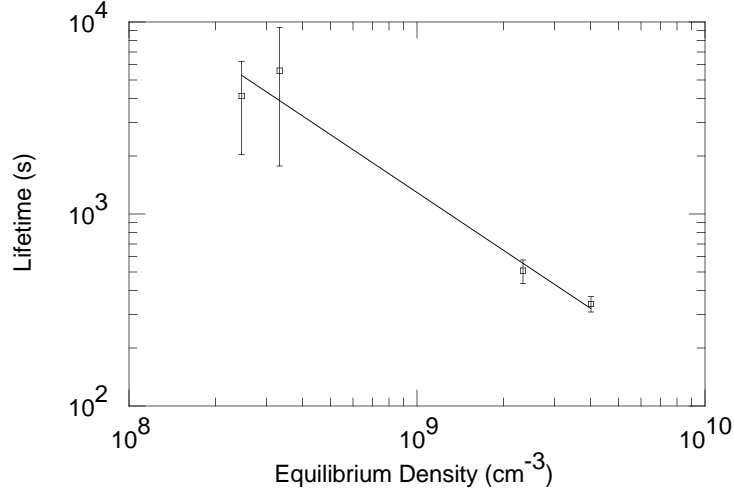

Figure 3. Electron plasma lifetime as a function of equilibrium density, determined from data in Fig. 2 for hold times greater than 100 s.

where B is the magnetic field, L is plasma length, P is neutral pressure, n is plasma density, and f is an undetermined function of plasma temperature. A fit to the LLNL data (Fig. 3) indicates a value of $a \approx 1$. Interpolating over several orders of magnitude in density and radius between UCSD data (5) and these preliminary LLNL data suggests $a \sim 1.5$. The CCD camera diagnostic is now fully on-line, and work is underway to further refine the trapping characteristics and scaling laws of this device.

POSITRON BEAM AND PULSED INJECTION

Positrons are injected into the trap from the LLNL Linac intense pulsed positron beam. (6) The positron beam is produced from the photon-electron-positron shower
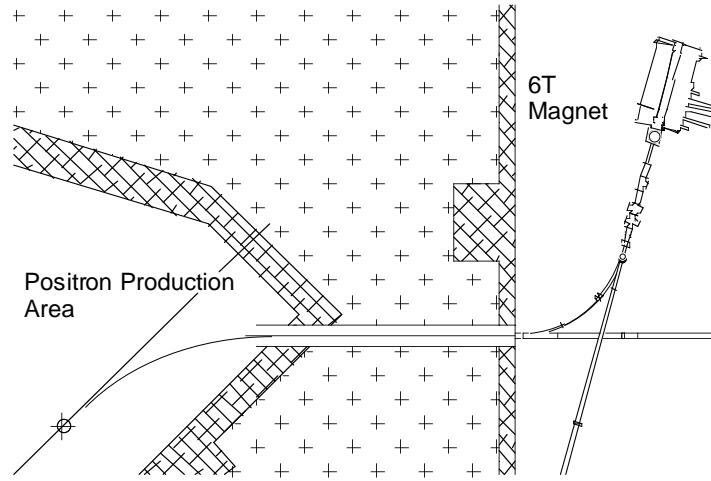
FIGURE 4. Diagram of the positron transport system.

generated by the 100 MeV electron beam in a tungsten converter target. High energy positrons are thermalized in a set of tungsten vanes, which have a negative work function for positrons, so those that diffuse to the vane surfaces are ejected with 1-2 eV. To preserve the 20 ns pulse width during transport through the solenoidal guide field to the trap (Fig. 4), the positrons are accelerated electrostaticly to ~6 kV. The positron flux, determined from the annihilation radiation at a beam stop just upstream of the trap, is 3×10^6 e$^+$/pulse. At the maximum Linac repetition rate of 1440 pulses/s, the beam intensity is 4.4×10^9 e$^+$/s.

The trapping scheme for accumulating positrons makes use of the pulsed nature of the positron beam. A 1000 Å tungsten remoderation foil at the front of the trap thermalizes the positrons, with ~20% efficiency, greatly enhancing the phase-space brightness of the beam by removing the large axial energy spread resulting from injection into the high magnetic field. The 1-2 eV positrons are then more easily captured in the trap. Trapping proceeds in two phases, the first by simple TOF (time-of-flight) capture, followed at higher positron densities by collisional cooling into the axial well. In the first phase, the remoderation foil, which is used as an electrostatic end cap, is dropped to ground potential for a time $\tau_g \geq \tau_p$, where τ_p is the width of the positron pulse. The positrons drift into the trap and spread evenly throughout the trapping region before the next pulse arrives. The fraction of trapped particles lost when a new pulse is injected is τ_g/τ_r, where τ_r is the round-trip travel time of positrons in the trap. The number of pulses trapped in this phase then asymptotically approaches τ_r/τ_g, at which point positrons are lost at the same rate at which they are injected.

The second phase of trapping occurs when the density of particles in the trap is high enough for collisions to equilibrate the transverse and longitudinal temperatures before the next pulse arrives (7). The trap is held at a negative bias, so as longitudinal energy is scattered into the transverse degrees of freedom the positrons cool into the axial potential well. Cyclotron radiation cools the transverse energy in less than a second. Once the positrons are in the potential well they can no longer escape when the front barrier is lowered. The transition to this second phase of trapping can be clearly seen in numerical simulations. For example, Figure 5 shows positron accumulation for the conditions in our first positron injection
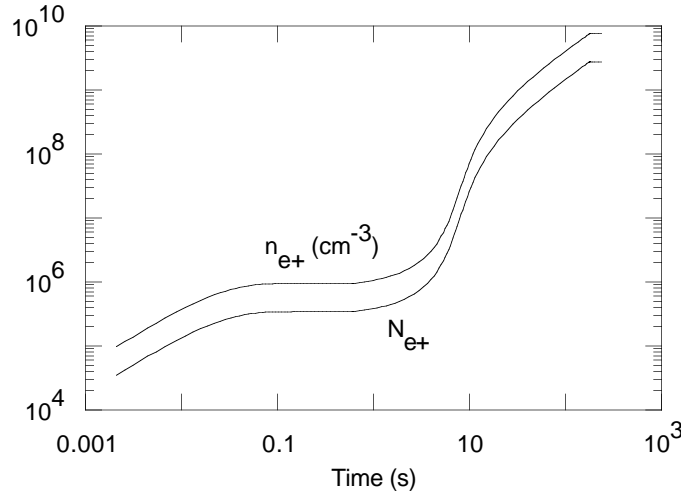
FIGURE 5. Numerical simulation of positron accumulation scheme. (L=46 cm, B=30 kG, well depth = 60 V, Linac rep. rate = 480 pps.)

experiments, described below. Under ideal conditions of injection and remoderation, ~9×10^7 positrons could be trapped per second.

FIRST RESULTS OF POSITRON INJECTION

The two major technical difficulties encountered in the first experiment were transport into the high-field region of the trap and remoderation of the positrons. As the positrons passed from the 150 G guide field into the 30 kG field used in the experiments presented here, magnetic mirroring gave an acceptance angle of less than five degrees. Irregularities in the guide field provided a transverse impulse to the positrons, resulting in a "spinning up" of the beam and consequent mirroring of the positrons. Refined techniques for operating the transport magnets improved transmission efficiency from an initial value of 1% to greater than 35%.

The unannealed tungsten foil used in the initial experiment gave only a 0.8% remoderation efficiency, instead of the expected 20%, when cooled to 77 K with the rest of the trap. Crystal defects in an unannealed foil inhibit positron diffusion to the surface. Cryopumping of impurities on the foil would inhibit re-emission. A recent experiment with an annealed foil at 300 K has improved performance to 5-6% remoderation. Cooling the bore with the annealed remoderation foil in place will show whether cryopumping is actually a problem requiring redesign of the remoderation stage.

These improvements resulted in 3.5×10^4 remoderated positrons injected into the trap per pulse. The round-trip flight time was 240 ns in this trap configuration. With an injection gate width of 25 ns, the TOF capture limit was about 3.5×10^5 positrons, achieved in a small fraction of a second. The actual accumulation of positrons as a function of hold time is shown in Figure 6. The fact that positrons continued to accumulate for up to 20 s indicates that particle cooling into the well was occurring. The time distribution of the charge signal as the trap was dumped indicates a significant accumulation of positrons near the bottom of the potential
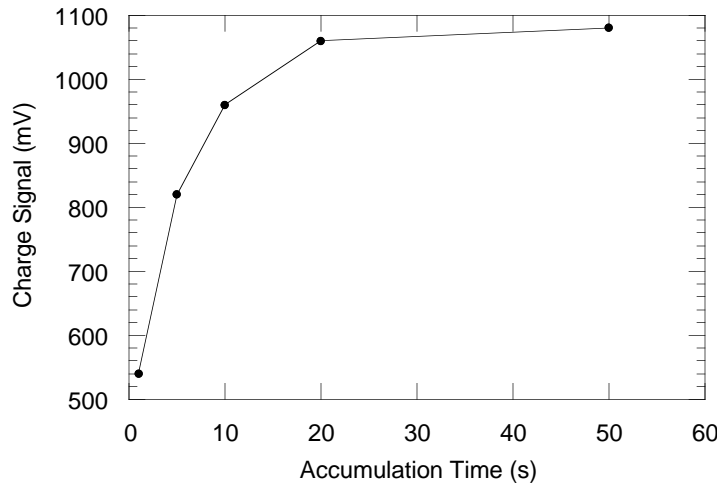
Figure 6. Charge dump signal on phosphor as a function of accumulation time.

well. Both the accumulation rate and the maximum density achieved scaled linearly with the repetition rate of the positron beam.

Calibration of the total number of positrons with the observed charge signal was complicated by saturation of the MCP. The relatively low repetition rate of one charge dump per 20 s made statistical counting from the annihilation gamma-ray signal also difficult. Three attempts at indirect calibration were made, using electron plasma diocotron measurements, the annihilation signal of single positron pulses, and the signal from a charge-sensitive pre-amp attached to the MCP with no voltage across the plate. Different calibrations give results ranging from $1.8x10^6$ to $2x10^7$ positrons trapped. Direct measurement of the number of trapped particles will be made in the next run by looking at the diocotron frequency of the positron column. The large number of positrons captured also allows use of the MCP at lower gain, which should reduce the problem of charge saturation.

An image of the dumped positron plasma is shown in Figure 7. The measured FWHM radius was 0.45 mm. The trapping region was 46 cm long, which gave a volume of approximately 0.29 cm^3, and a density of at least $6x10^6$ cm^{-3} and possibly as high as $6x10^7$ cm^{-3}.*

A comparison of the data of Figure 6 and calculations of Figure 5 reveals several important results regarding positron accumulation and confinement. Initially, the trap was filling too quickly to be accounted for by positron collisions alone. For example, the calculated density at 1s is 10^6 cm^{-3}, but the actual accumulation was at least three times that value. The accumulation should continue linearly throughout this range, but the results show saturation, while CCD images indicated no radial transport. This implies a large effect from collisions with neutral particles, enhancing early collisional cooling into the well and causing positron loss due to annihilation or positronium formation on a time scale of a few seconds. This data is consistent with the early results of Surko *et. al.* (8). Experiments to improve

---

* An abstract for a poster session at the annual meeting of the APS Division of Plasma Physics mistakenly suggested that design-goal densities of 10^{10} cm^{-3} had actually been achieved. We apologize for the error.
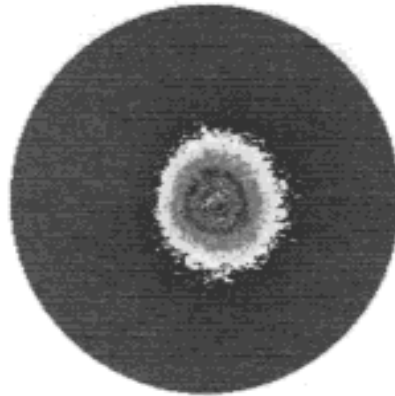
Figure 7. CCD Image of positron column. FWHM radius is 0.45 mm

confinement by cooling the trap are in preparation. If surface contamination of the remoderation foil proves not to be a limiting factor, we expect to achieve significantly higher densities in the near future.

ACKNOWLEDGMENTS

REFERENCES

(1) Cowan, T. E., Howell, R. H., Rohatgi, R. R., and Fajans, J., *Nuc. Inst. and Methods B*, **56-7**, 599–603 (1991).

(2) Driscoll, C. F., and Malmberg, J. H., *Phys. Rev. Let.*, **50**, 167–170 (1983).

(3) Malmberg, J. H., and Driscoll, C. F., *Phys. Rev. Let.*, **44**, 654–657 (1980).

(4) Peurrung, A. J., and Fajans, J., *Phys. Fluids B*, **1**, 2073–2084 (1989).

(5) Cass, A., contribution, this conference.

(6) Howell, R. H., Rosenberg, I. J., and Fluss, M.J., *Applied Physics A*, **43**, 247–255 (1987).

(7) Beck, B. R., Fajans, J., and Malmberg, J. H., *Phys. Rev. Let.*, **68**, 317–320 (1992).

(8) Surko, C.M., Leventhal, M., Passner, A., and Wysocki, F.J., "A Positron Plasma in the Laboratory – How and Why", *Proceedings of the ONR Conference on Non-Neutral Plasmas*, 1988, pp. 185–200.